Langmuir

ARTICLE

pubs.acs.org/Langmuir

Temperature Driven Annealing of Perforations in Bicellar Model Membranes

Mu-Ping Nieh,[†] V. A. Raghunathan,[‡] Georg Pabst,[§] Thad Harroun,[∥] Kazuomi Nagashima,[⊥] Hannah Morales,[⊥] John Katsaras,[#,▽] and Peter Macdonald*[,⊥]

[†]Chemical, Materials and Biomolecular Engineering Department, Institute of Material Sciences, University of Connecticut, 97 North Eagleville Road, Storrs, Connecticut 06269-3136, United States

[‡]Raman Research Institute, Bangalore 560 080, India

[§]Institute of Biophysics and Nanosystems Research, Austrian Academy of Sciences, Schmiedlstrasse 6, A-8042 Graz, Austria

[∥]Department of Physics, Brock University, St. Catherines, Ontario L2S 3A1, Canada

[⊥]Department of Chemistry, University of Toronto, and Department of Chemical and Physical Sciences, University of Toronto Mississauga, 3359 Mississauga Road North, Mississauga, Ontario L6J 1J9, Canada

[#]Oak Ridge National Laboratory, Neutron Sciences Directorate, Oak Ridge, Tennessee 37831-6475, United States

[▽]National Research Council, Canadian Neutron Beam Centre, Chalk River, Ontario K0J 1J0, Canada

ABSTRACT: Bicellar model membranes composed of 1,2-dimyristoylphosphatidylcholine (DMPC) and 1,2-dihexanoylphosphatidylcholine (DHPC), with a DMPC/DHPC molar ratio of 5, and doped with the negatively charged lipid 1,2-dimyristoylphosphatidylglycerol (DMPG), at DMPG/DMPC molar ratios of 0.02 or 0.1, were examined using small angle neutron scattering (SANS), ^{31}P NMR, and ^{1}H pulsed field gradient (PFG) diffusion NMR with the goal of understanding temperature effects on the DHPC-dependent perforations in these self-assembled membrane mimetics. Over the temperature range studied via SANS (300−330 K), these bicellar lipid mixtures exhibited a well-ordered lamellar phase. The interlamellar spacing *d* increased with increasing temperature, in direct contrast to the decrease in *d* observed upon increasing temperature with otherwise identical lipid mixtures lacking DHPC. ^{31}P NMR measurements on magnetically aligned bicellar mixtures of identical composition indicated a progressive migration of DHPC from regions of high curvature into planar regions with increasing temperature, and in accord with the "mixed bicelle model" (Triba, M. N.; Warschawski, D. E.; Devaux, P. E. *Biophys. J.* **2005**, *88*, 1887−1901). Parallel PFG diffusion NMR measurements of transbilayer water diffusion, where the observed diffusion is dependent on the fractional surface area of lamellar perforations, showed that transbilayer water diffusion decreased with increasing temperature. A model is proposed consistent with the SANS, ^{31}P NMR, and PFG diffusion NMR data, wherein increasing temperature drives the progressive migration of DHPC out of high-curvature regions, consequently decreasing the fractional volume of lamellar perforations, so that water occupying these perforations redistributes into the interlamellar volume, thereby increasing the interlamellar spacing.

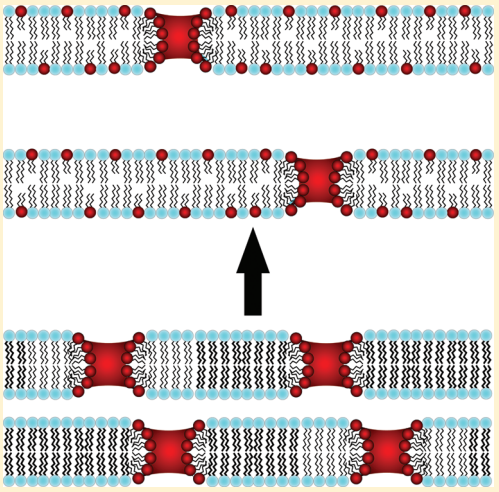

INTRODUCTION

Bicellar mixtures continue to attract attention due to their considerable advantages as model membrane systems, as described in a multitude of review articles.[1−12] They consist of mixtures of short-chain and long-chain amphiphiles,[13,14] as typified by the canonical mixture of dihexanoylphosphatidylcholine (DHPC) and dimyristoylphosphatidyl choline (DMPC) introduced by Sanders and Shwonek.[15] The DMPC assembles into a planar bilayer stabilized at its edges by a coating of DHPC. The popularity of bicellar mixtures stems in large part from their propensity to align in a magnetic field, a result of their inherent diamagnetic susceptibility anisotropy: a property which renders them extremely useful as biomembrane mimics for solid state[16−36] and solution state[37−42] nuclear magnetic resonance (NMR) studies of membrane proteins and membrane-associating biomolecules,[43−55] and as an orienting medium for NMR structural studies of soluble proteins and nucleic acids.[56−68]

The structures into which bicellar mixtures self-assemble display considerable morphological plasticity. At least three major influences have been identified, with these being (1) the

Received: November 29, 2010
Revised: February 25, 2011
Published: March 25, 2011

molar ratio, Q, of long-chain to short-chain amphiphiles, (2) the lipid/water ratio, and (3) the temperature. From results obtained with a host of physical techniques, including electron microscopy (EM),[69−71] fluorescence spectroscopy,[72] NMR,[73−76] small angle X-ray scattering (SAXS),[77] and small angle neutron scattering (SANS),[8,77−82] the following general, if not universal, consensus has emerged. At low Q, or at low lipid concentrations, or at temperatures below the DMPC gel-to-liquid-crystalline phase transition (T_m), bicellar mixtures do not magnetically align and appear discoidal with DHPC occupying the edges of a DMPC bilayer disk, as per the "ideal" bicelle model.[83] At higher Q and higher lipid concentration and at temperatures above the T_m of DMPC, the morphology evolves to a magnetically alignable nematic phase consisting of lamellar structures far larger in dimension than contemplated by the ideal bicelle model, presumably stabilized by a coating of DHPC at the edges.

Using SANS, the morphology of the magnetically alignable nematic phase of canonical DMPC/DHPC bicellar mixtures has been characterized as consisting of single-bilayer-thickness ribbon-like aggregates,[80,81] a result confirmed by cryo-transmission EM[70] and, recently, NMR.[84] However, when such bicellar mixtures contain the negatively charged phospholipid DMPG, a swollen lamellar phase is observed by SANS.[78] Such a lamellar phase is also observed upon adding small amounts of lanthanide ions, such as Tm^{3+} or Yb^{3+}, which bind with high affinity to the phosphates of the constituent phospholipids.[85] The presence of surface-bound lanthanides also induces a realignment of the bilayer normal, from its spontaneous orientation perpendicular to the applied magnetic field to one that is parallel, with this being directly the result of the positive magnetic susceptibility anisotropy introduced upon lanthanide binding.[86,87] This smectic phase was proposed to consist of perforated "Swiss cheese"-like lamellae,[86] a morphology confirmed by SANS experiments[78,87] and supported by electron paramagnetic resonance[88] and NMR measurements.[89,90]

The role of charge in influencing the morphology of bicellar mixtures is clearly pivotal but, for the most part, not well understood. In addition to those features noted above, adding charged species to bicellar mixtures has been shown to improve the stability and the quality of alignment of the resultant self-assembly in an external magnetic field.[91,92] However, these charged bicellar mixtures exhibit complex SANS diffraction patterns which are not easily interpreted.[93]

In order to better understand how surface charge affects the lamellar phase of bicellar mixtures, we report here the use of a combination of SANS and NMR measurements to examine temperature effects on a DMPC/DHPC bicellar mixture containing added DMPG at several molar ratios R = DMPG/DMPC. SANS provides a number of useful morphological parameters including, in particular for the present purposes, the bilayer thickness and the lamellar repeat spacing.[8] ^{31}P NMR provides a means to assess the quality of magnetic alignment of the bicellar mixture, as well as the equilibrium distribution of DHPC between planar and edge regions.[94] Diffusion NMR can be a useful probe of bicellar morphology[89,90] and, in the current context, via measurements of the transbilayer diffusion of water in bicellar mixtures, provides the means to evaluate the degree of lamellar perforation.[95]

MATERIALS AND METHODS

Sample Preparation. DMPC (1,2-dimyristoylphosphatidylcholine), DHPC (1,2-dihexanoylphosphatidylcholine), and DMPG (1,2-dimyristoylphosphatidylglycerol) were purchased from Avanti Polar Lipids (Alabaster, AL) and were used without further purification.

For SANS measurements, lipid mixtures of DMPC and DHPC were prepared, having a constant molar ratio DMPC/DHPC = 5, to which DMPG was added at molar ratios of R = DMPG/DMPC = 0.02 and 0.1. The dry lipid powders were hydrated in D_2O (99.9% purity, Chalk River Laboratories) to a total lipid concentration, C_L, of 20 wt % and dispersed by cycling between low (∼277 K) and high (∼323 K) temperatures in combination with vortex mixing.[86,87] Another set of samples lacking DHPC was prepared for SANS, wherein pure DMPC was mixed with DMPG at the same R values as above, this time using methanol as the solvent. The solvent was then removed under a stream of dry air while keeping the sample at ∼333 K, and the sample was subsequently placed under vacuum for several hours to remove any remaining traces of methanol. The resulting dry lipid film was hydrated and dispersed in D_2O to a C_L of 20 wt % following the same procedure as the samples with DHPC.

For NMR measurements, dry lipid mixtures of DMPC, DMPG, and DHPC were prepared, having a constant molar ratio (DMPC + DMPG)/DHPC ≈ 5, with DMPG present at molar ratios of R = DMPG/DMPC = 0.02 and 0.1. The dry lipid powders were dispersed in a volume of 1:1 (v/v) H_2O/D_2O containing $YbCl_3$ sufficient to achieve a Yb^{3+}/lipid ratio of 1/75 and a total lipid concentration, C_L, of 20 wt %. These mixtures were then subjected to essentially the same temperature cycling and vortexing procedure described above for SANS samples. Yb^{3+} was included in order to achieve the positive magnetic alignment desired for conducting NMR diffusion measurements of transbilayer water diffusion.

Small Angle Neutron Scattering. Both neutron scattering and X-ray diffraction are capable of obtaining lamellar spacings and resolving the density profile across lipid bilayers. Neutrons were used here for two reasons: (1) to avoid potential sample damage from exposure to high energy X-rays, and (2) because the oscillating-flow cell with the correct geometry is available commercially. Neutron scattering experiments were carried out at the National Research Universal (NRU) reactor (Chalk River Laboratories, Canada) using either the N5 or E3 diffractometer. At N5, the (002) reflection of a pyrolytic-graphite monochromator was used to select 2.37 Å wavelength (λ) neutrons, whereas at E3 λ = 2.327 Å neutrons were obtained using the (113) reflection of a germanium monochromator. At N5, an additional pyrolytic-graphite filter was used to suppress the higher energy harmonics scattered by the (002) reflection.

Samples were transferred into rectangular flow cells of dimensions 0.05 × 1.0 × 4.0 cm^3 (Starna Cells, Inc.) at 277 K, a temperature where the samples exhibit low viscosity. The sample cell was sandwiched between two aluminum blocks, whose temperature was controlled via a circulating water bath.[81] An oscillating shear flow along the sample cell's long axis (4.0 cm) was applied when the samples were heated to T ∼ 323 K, aligning the bilayer normals perpendicular to the major face (1.0 × 4.0 cm^2) of the flow cell. After shearing, the bilayers remained aligned for several days.

The incident monochromatic neutron beam impinged on the 0.05 × 4.0 cm^2 face of the sample cell. Samples were equilibrated at each temperature for 30 min prior to exposure. Diffraction experiments covered wave vector transfers $q = 4\pi \sin(\theta)/\lambda$ from 0.03 to 0.26 $Å^{-1}$, where 2θ is the scattering angle. However, because of a strong refraction peak interference at 0.19 $Å^{-1}$, possibly arising from material (quartz) in the shear cell, the maximal q was truncated at ∼0.17 $Å^{-1}$. The $\Delta\lambda/\lambda$ was less than 2% for the monochromators. Both incident (before sample) and diffracted (after sample) beams were collimated with a channel (19 in. length × 1/10 in. width × 1 in. height), resulting in a total resolution of $\Delta q/q$ ∼ 30% at q = 0.03 $Å^{-1}$ and ∼5% at q = 0.17 $Å^{-1}$.

From SANS diffraction patterns versus q, the average separation, d, of the lamellae can be readily derived through a linear regression,

$$q_h = \frac{2\pi}{d} h \quad (1)$$

dx.doi.org/10.1021/la104750x |Langmuir 2011, 27, 4838–4847

where h is the order of diffraction and q_h is the center of the hth Bragg peak, determined by fitting a Gaussian distribution.

For reasons to be discussed later, the bilayer thickness, d_B, of bilayers containing DHPC could not be accurately estimated using the usual relation $d = d_B/\phi_l$, where ϕ_l is the lipid volume fraction.[96] Therefore, d_B of these systems was estimated by defining a model for the scattering length density (SLD) profile normal to the bilayers. Recently, Kučerka et al. have reported on several SLD models with varying complexities.[97] As a result of the limited q-space sampled, and the need to keep the number of adjustable parameters to a minimum (see below), we used a slab SLD profile described by

$$\mathrm{SLD}(z) = \begin{cases} \Delta b & -\frac{1}{2}d_B < z < +\frac{1}{2}d_B \\ 0 & \text{otherwise} \end{cases} \quad (2)$$

where Δb is the difference between the mean lipid SLD and that of D_2O. Fourier transforming eq 2 produces the theoretical bilayer form factor $F(q)$ as a continuous function of q.

$$F(q) = 2\Delta b \frac{\sin(qd_B/2)}{q} \quad (3)$$

The intensity scattered by a single bilayer is given by

$$I(q) \propto \frac{|F(q)|^2}{q} \quad (4)$$

where $1/q$ is the standard Lorentz correction factor for aligned samples. In the case of a stack of bilayers, as in the present experiment, the one-dimensional Fourier transform is sampled at discrete q values. Explicitly, the experimental form factor, F_h, for each Bragg reflection is given by the square root of the integrated peak intensity, obtained from a Gaussian fit, multiplied by the corresponding value of q (see eq 4), so that d_B may be determined by fitting eq 3 to the $|F_h|^2$. It should be noted that the signal/background ratio was >3 even in the worse case and that the background intensity was assumed to follow a q^{-2} dependence.

An alternative method for estimating d_B would be to calculate the SLD profile through a Fourier synthesis as follows,

$$\mathrm{SLD}(z) = \sum_{h=1}^{h_{max}} \alpha_h |F_h|^2 \cos(2\pi hz/d) \quad (5)$$

where $\alpha_h = \pm 1$ is the phase factor. However, when the number of quasi-Bragg peaks is limited, as in most cases here, and when these peaks have the same phase, as they do here since $d > 100$ Å, there are strong Fourier truncation artifacts, making it difficult to determine the bilayer/water interface from the calculated SLD profiles. In contrast, eq 3 requires only two adjustable parameters, so that even when a limited number of Bragg reflections is available, reasonable estimates of d_B are possible. Note that, because of the low resolution SLD model used, the d_B values obtained are not absolute values.[97,98] Thus, our emphasis is on the relative changes of d_B as a function of temperature.

Nuclear Magnetic Resonance Spectroscopy. Bicellar mixtures prepared as above were transferred into a 5 mm NMR sample tube at 277 K and placed in the bore of a 500 MHz NMR spectrometer. The sample temperature was then raised to 308 K. An annealing procedure was carried out involving repeated cycling of the temperature between 293 and 308 K with 10−15 min of equilibration at either extreme to encourage magnetic alignment. The quality of the magnetic alignment was assessed via ^{31}P NMR spectroscopy.

All NMR spectra were recorded on a Varian Infinity 500 MHz NMR spectrometer using a Varian 5 mm double resonance liquid probe equipped with gradient coils along the z-direction. The sample temperature was controlled to the desired value ± 0.5 K, as calibrated separately using ethylene glycol.[99]

^{31}P NMR spectra were recorded at 202.31 MHz using a single pulse excitation, quadrature detection, complete phase cycling of the pulses, and WALTZ proton decoupling during the signal acquisition with a proton decoupler field strength of 2 kHz. Typical acquisition parameters are as follows: a 90° pulse length of 25 μs, a recycle delay of 3 s, a spectral width of 100 kHz, and an 8k data size. Spectra were processed with an exponential multiplication equivalent to 50 Hz line broadening prior to Fourier transformation and were referenced to 85% phosphoric acid.

^{1}H NMR diffusion measurements were performed at 499.78 MHz using the stimulated echo (STE) pulsed field gradient (PFG) procedure,[100] with square gradient pulses of constant duration (5 ms) and variable gradient pulse amplitude, directed along the longitudinal (z) axis exclusively. Typical acquisition parameters are as follows: a 90° pulse length of 16 μs, a spin echo delay of 10 ms, a stimulated echo delay between 100 and 1000 ms, a recycle delay of 5 s, a spectral width of 10 kHz and a 4K data size. The phases of the radio frequency pulses were cycled to eliminate unwanted echoes.[101] Spectra were processed with an exponential multiplication equivalent to 5 Hz line broadening prior to Fourier transformation and were referenced to tetramethylsilane (TMS). Gradient strength was calibrated from the known diffusion coefficient of HDO at 25 °C.[102] Proton T_1 relaxation times were measured using a standard inversion recovery protocol.

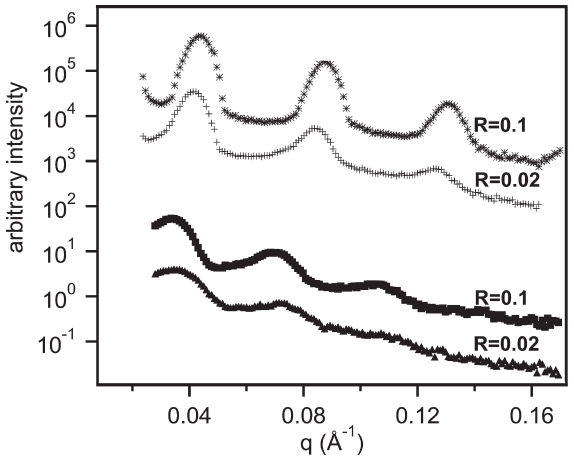

Figure 1. Neutron diffraction data for DMPC/DHPC/DMPG mixtures ($Q = 5$, $R = 0.02$ (+) or 0.1 (∗), $C_l = 20$ wt %) and DMPC/DMPG mixtures ($R = 0.02$ (▲) or 0.1 (■), $C_l = 20$ wt %) at 304 K. Data have been shifted vertically for better visualization of the individual scattering patterns.

RESULTS AND DISCUSSION

Small Angle Neutron Scattering. Figure 1 shows the SANS patterns for all samples equilibrated at 304 K. Up to three orders of quasi-Bragg reflections, indicating one-dimensional lamellar order, can be distinguished. The scattering contrast for lipid mixtures containing DHPC was significantly higher than for those without, most probably due to superior alignment in the presence of DHPC.

Qualitatively, the interlamellar spacing d is inversely related to the position of the quasi-Bragg reflections. Thus, Figure 1 shows that for DMPC/DMPG mixtures, d was practically identical for the $R = 0.1$ and 0.02 samples. Likewise, for the DMPC/DHPC/DMPG mixtures, differences in the lamellar spacing d for the $R = 0.1$ and 0.02 cases were minor.

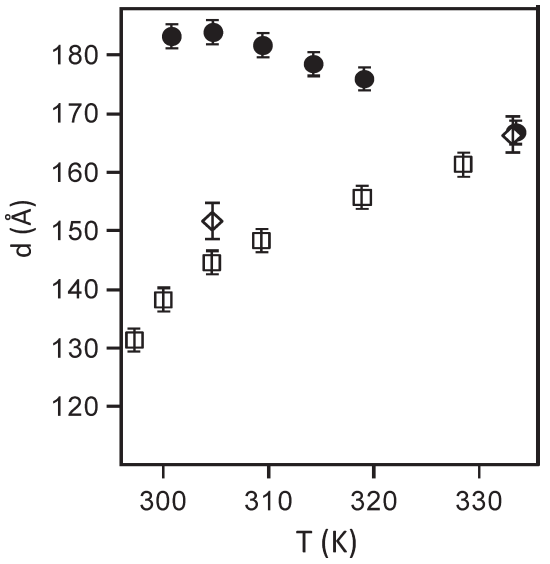

Figure 2. Interlamellar spacing, d, as a function of temperature for the DMPC/DMPG mixture with R = 0.1 (●) and the DMPC/DHPC/DMPG mixtures with R = 0.1 (□) or R = 0.02 (◇). Values for the R = 0.02 sample (data not shown) were similar to those for the R = 0.1 sample for the DMPC/DMPG mixture.

Quantitatively, eq 1 is employed to extract the interlamellar spacing d. Figure 2 shows the temperature dependence of d for the DMPC/DMPG, R = 0.1 mixture and for the DMPC/DHPC/DMPG, R = 0.02 and 0.1 mixtures. It is evident that the interlamellar spacing is smaller when DHPC is present than when it is absent, at all but the highest temperatures. The DMPC/DMPG mixture lacking DHPC displayed a monotonic decrease of d with increasing temperature. For the latter mixture, the bilayer thickness d_B can be estimated simply using the relation, $d = d_B/\Phi_l$, where Φ_l is the volume fraction of lipid.[96] One finds that d_B gradually decreases from ~36 Å at 300 K to ~33 Å at 333 K. Such values are comparable to those reported in the literature for both DMPC/DMPG[78,79] and pure DMPC bilayers.[98] The gradual thinning of the bilayer with increasing temperature is the result expected given the corresponding increase in the probability of trans−gauche isomerizations along the hydrocarbon chains of the lipid molecules.[103,104]

In contrast, the DHPC-containing DMPC/DMPG mixtures exhibit an increase of d with increasing temperature. Estimating the bilayer thickness d_B of these DHPC-containing mixtures directly from the raw diffraction data using $d = d_B/\Phi_l$, as above, given the volume fraction of lipid Φ_l, yields values of d_B on the order of 23−25 Å. Such values of the bilayer thickness are much smaller than those previously reported for the same system, where a d_B value of ~32 Å was determined from an analysis of SANS data for DMPC/DHPC unilamellar vesicle dispersions.[78,79,105,106] Moreover, and in further contrast to the behavior of DMPC/DMPG mixtures lacking DHPC, this method of analysis uncritically applied yields an apparent increase of d_B with increasing temperature, from ~23 Å at 300 K to ~25 Å at 333 K, for DMPC/DMPG mixtures containing DHPC.

In order to better estimate d_B for the DHPC-containing mixtures, we applied the protocol described in the Materials and Methods, wherein eq 3 is fit to experimental form factors $|F_h|^2$, assuming a specific model for the scattering length density perpendicular to the bilayer. Figure 3 shows a typical fit, for the

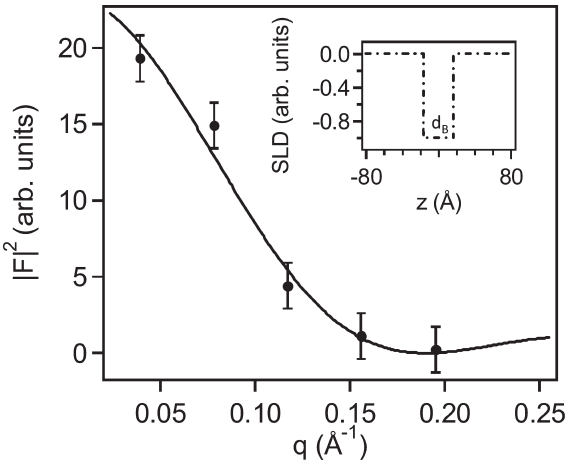

Figure 3. Lorentz corrected Bragg peak intensities (●) for the R = 0.1 DMPC/DHPC/DMPG mixture at 328 K. The solid line is a fit of eq 3 to the data, yielding d_B = 33 ± 1 Å. The inset to the figure shows the corresponding SLD profile.

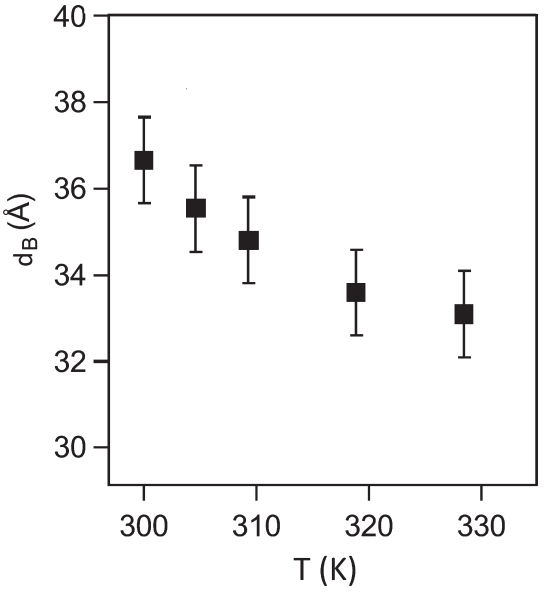

Figure 4. Temperature dependence of the membrane thickness d_B for the R = 0.1 DMPC/DHPC/DMPG (■) mixture.

particular case of the DMPC/DHPC/DMPG (R = 0.1) mixture at 328 K, yielding d_B = 33 ± 1 Å, a value in good agreement with the bilayer thickness of DMPC/DHPC unilamellar vesicles reported in the literature,[35,36,61,62] and comparable to the values of d_B for DMPC/DMPG mixtures reported here. When evaluated in this fashion as a function of temperature, as shown in Figure 4, it is evident that, despite the simplicity of the scattering density model used, likewise for DMPC/DHPC/DMPG mixtures, increasing temperature produces bilayer thinning.

Since for all systems d_B decreases with increasing temperature, the contra-variant temperature dependence of the interlamellar spacing d in DMPC/DMPG versus DMPC/DHPC/DMPG mixtures must be due to differences in the temperature dependence of the average interbilayer separation, $d_W = d - d_B$.

One factor influencing the interlamellar spacing is increased thermal undulations of the bilayers at higher temperatures.

dx.doi.org/10.1021/la104750x |Langmuir 2011, 27, 4838–4847

Thermal undulations of bilayers result in an excess bilayer area ΔA, given by,

$$\frac{\Delta A}{A} = \frac{k_B T}{4\pi\kappa} \ln\left(\frac{q_{max}}{q_{min}}\right) \quad (6)$$

where A is the projected area of the bilayer, T is the temperature, κ is the bending rigidity of the bilayer, and q_{max} and q_{min} are the high and low wavelength cutoffs, respectively.[107,108] The dependence of d on lipid volume fraction, Φ_L, is then given by,

$$d = \frac{d_B}{\phi_L}\left(1 + \frac{\Delta A}{A}\right) \quad (7)$$

so that, in the limit of very high κ, $\Delta A \rightarrow 0$ and d attains its minimum possible value, d_{min}, for a given Φ_L. However, in the case of highly flexible bilayers, $\Delta A/A$ is non-negligible so that not only can d be significantly larger than d_{min},[109] but, since ΔA is directly proportional to T, d can increase with T. On the other hand, increasing the surface charge density σ in otherwise flexible bilayers, such as surfactant systems with $\kappa \sim k_B T$, gradually stiffens the bilayers, thereby decreasing ΔA and producing lower values of d.[110,111] In the systems investigated here (i.e., $\kappa \sim 20 k_B T$), thermal undulations should not significantly affect d.[112] Moreover, the surface charge density arising from the presence of DMPG should further increase bilayer rigidity.[113−116] Thus, we do not consider thermal undulations to be the likely cause of the observed increase of d with increasing temperature for the DMPC/DHPC/DMPG mixtures.

Another possible explanation for the increase of d with increasing temperature observed in DMPC/DHPC/DMPG mixtures is a progressive annealing of porelike defects in the bilayers. At low temperatures, such bicellar mixtures display an isotropic phase made up of diskoidal assemblies consisting of DMPC/DMPG-rich planar regions edged by a DHPC-rich coating. At higher temperature, the disks fuse into extended lamellar sheets perforated by DHPC-lined pores.[78,79,81] Similar behavior is observed in zwitterionic bicellar mixtures of DMPC and DHPC, with one difference being that the disks first fuse into a nematic phase of ribbonlike structures before forming lamellae.[78,79] The formation of ribbons and lamellae can be rationalized by assuming a gradual decrease in the DHPC available to stabilize edge regions due to an increased miscibility of DHPC with DMPC at higher temperatures.[94] Consequently, once the lamellar morphology is achieved, further temperature increases reduce the number and/or size of the DHPC-lined pores, effectively squeezing out the water that once occupied the holes. Since these mixtures are not under excess water conditions, the "squeezed-out" water must find its way between the lamellae, giving rise to larger d values with increasing temperature.

The SANS data provide an indication that such an effect is indeed occurring. Specifically, the fractional area of the bilayers occupied by pores, f_{pores}, can be estimated from the relation $f_{pores} = (d_{min} - d)/d_{min}$, where d_{min}, the lamellar repeat spacing for ideally flat, defect-free bilayers, is given by d_B/Φ_L in eq 7. Figure 5 shows the variation of f_{pores} with temperature, where the trends clearly support the notion that the pores are annealing at higher temperatures. Note that the calculation of Φ_L assumes that essentially all the DHPC is resident within the self-assembly and not partitioned into the water: an assumption which is valid under these conditions to within a few percent of the total DHPC content.[94]

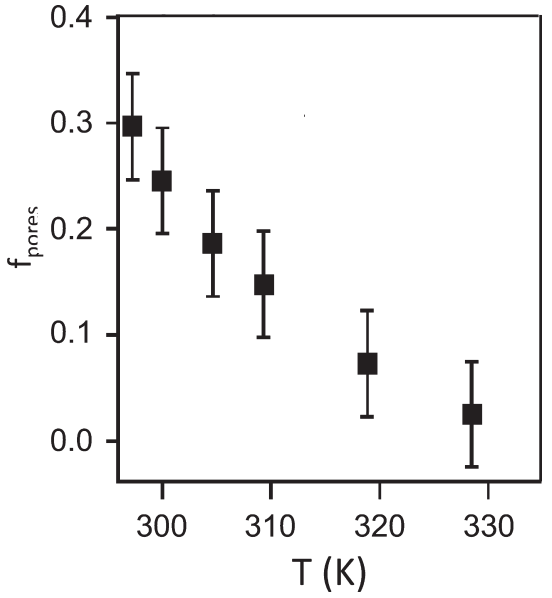

Figure 5. Estimated bilayer pore fraction, f_{pores}, from SANS analysis of the DMPC/DHPC/DMPG mixture at $R = 0.1$ (■).

Nuclear Magnetic Resonance Spectroscopy. The annealing of DHPC-lined pores with increasing temperature indicated by the SANS data described above can be examined independently using NMR. Figure 6 shows a series of ^{31}P NMR spectra of a positively magnetically aligned DMPC/DHPC/DMPG (Q = 5.0, R = 0.1) mixture at various temperatures. At 298 K, near the gel-to-liquid crystalline phase transition temperature of DMPC (and DMPG), the spectrum consists of a narrow isotropic component, assigned to DHPC, superimposed on a broad powder pattern, assigned to DMPC+DMPG. The fact that a powder spectrum is observed indicates that this bicellar mixture has not yet aligned in the magnetic field of the NMR spectrometer. Once the temperature increases significantly, however, one observes that the DMPC+DMPG powder component narrows, yielding a resonance centered at roughly 20 ppm. (Note that the isotropic and anisotropic chemical shifts of DMPC and DMPG are too similar to be resolved under these conditions.) This is behavior indicative of positive magnetic alignment, as expected in the presence of Yb^{3+}, wherein the normal to the bilayer plane is oriented parallel to the direction of the magnetic field. From the integrated peak areas, one may calculate the relative amounts of DMPC+DMPG versus DHPC. For the specific case of the R = 0.1 sample shown in Figure 6, the apparent mole fraction of DHPC present is X_{DHPC} = 0.176. The R = 0.1 sample employed for SANS measurements had an ostensible DHPC mole fraction of X_{DHPC} = 0.154. As will be discussed below, this small difference in the composition of the NMR versus SANS samples is of little importance when comparing SANS and NMR results for f_{pore}.

With increasing temperature, the frequency of the DHPC resonance shifts progressively toward that of DMPC+DMPG. Triba et al.[94] have interpreted such observations in terms of their "mixed bicelle model" in which DHPC at lower temperatures resides almost exclusively within highly curved edge regions of the bicellar assemblies, hence its isotropic ^{31}P NMR resonance position, but becomes progressively more miscible with DMPC (and DMPG) upon increasing temperature. Assuming fast

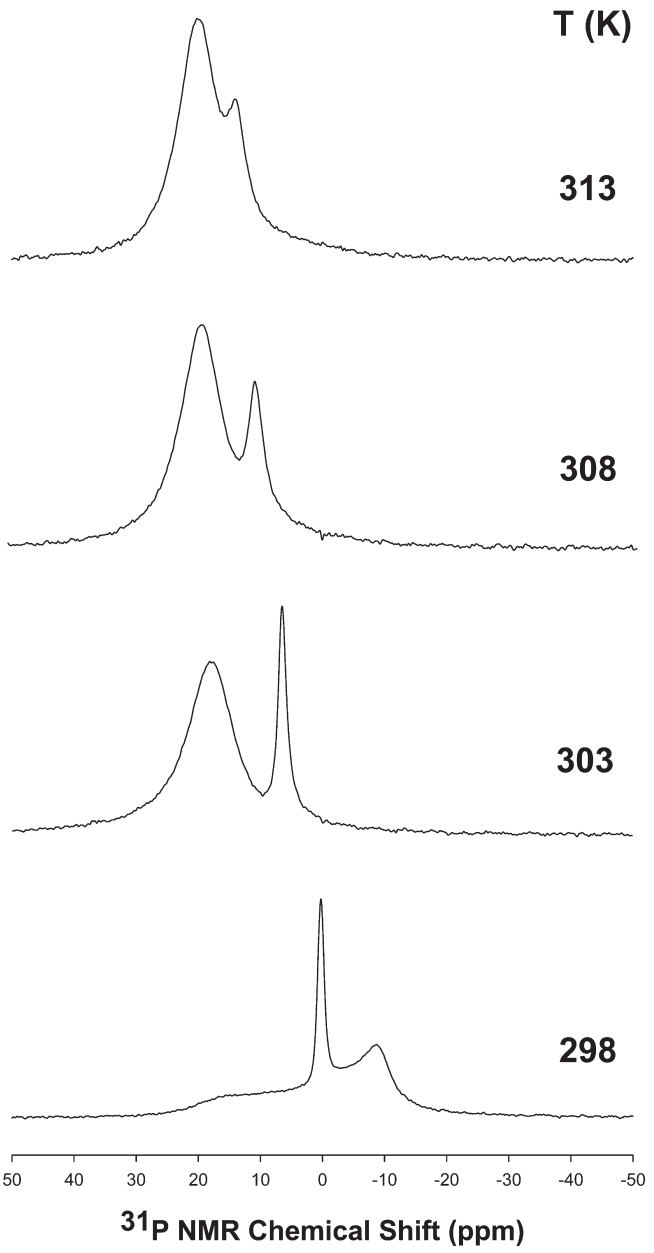

Figure 6. Temperature dependence of ^{31}P NMR spectra from a $Q = 5.0$, $R = 0.1$ DMPC/DHPC/DMPG mixture containing $YbCl_3$ at a Yb^{3+}/lipid ratio of 1/75 to produce positive magnetic alignment of the bicellar mixtures.

exchange of DHPC between edge and planar regions of the bicellar assembly, the observed frequency of the DHPC ^{31}P NMR resonance then reflects the equilibrium distribution of DHPC between these two environments. With the simplifying assumptions that the long-chain lipids DMPC and DMPG never occupy highly curved regions, and that the ^{31}P NMR isotropic and anisotropic chemical shifts of DMPC and DHPC are identical in the two environments, one may calculate an effective fractional population of DHPC occupying planar regions, ω^*, from the observed chemical shifts of DHPC (ω_{DHPC}) and DMPC+DMPG (ω_{DMPC}) via eq 8.

$$\omega^* = \frac{\omega_{DHPC}}{\omega_{DMPC}} \qquad (8)$$

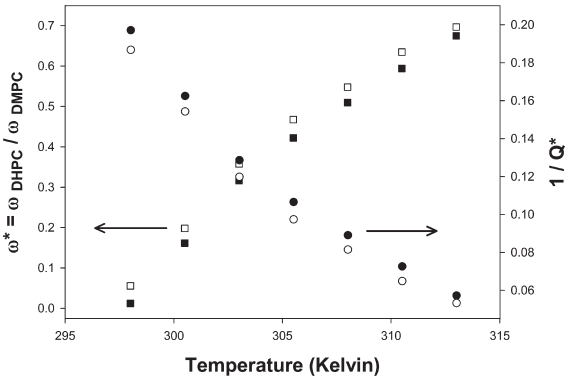

Figure 7. Fraction of DHPC resident in lamellar regions ($\omega^* = \omega_{DHPC}/\omega_{DMPC}$) (squares) and the proportion of edge versus lamellar lipids ($1/Q^*$) (circles) as derived from ^{31}P NMR chemical shifts for DMPC/DHPC/DMPG mixtures at $Q = 5.0$ and $R = 0.02$ (closed symbols) and 0.10 (open symbols), as a function of temperature.

The results of such a calculation are shown in Figure 7 for the two DMPG compositions, $R = 0.02$ and 0.10, relevant for comparison with SANS results. Evidently, DHPC progressively migrates from edge into planar regions of the bicelles with increasing temperature for both DMPG contents. Other DMPG compositions were investigated, specifically $R = 0.05$ and 0.15, and showed essentially identical effects. Note that increasing the DMPG content introduces surface charges which stiffen the bilayer and reduce thermal undulations. The resulting increase in the bicellar order parameter, $S_{bicelle}$, produces an increased residual chemical shift anisotropy for both DMPC and DHPC such that both ω_{DHPC} and ω_{DMPC} increase. By taking the ratio $\omega^* = \omega_{DHPC}/\omega_{DMPC}$, eq 8 compensates for this ordering effect of DMPG. As shown in Figure 7, ω^* is virtually independent of the R value, indicating that DMPG content does not particularly influence the equilibrium distribution of DHPC between planar and edge regions, at least over this range of DMPG compositions.

Further to this effect, one may calculate from the observed ^{31}P NMR chemical shifts the quantity Q^* relating the ratio of planar-to-edge lipids as per eq 9,

$$Q^* = \left[\frac{Q + \omega^*}{1 - \omega^*}\right] \qquad (9)$$

where, again, Q = (DMPC+DMPG)/DHPC, $\omega^* = \omega_{DHPC}/\omega_{DMPC}$, and ω_{DHPC} and ω_{DMPC} are the observed chemical shifts of DHPC and DMPC+DMPG, respectively. The inverse quantity, $1/Q^*$, then represents the ratio of total lipid available to form edge regions versus the total lipid forming planar regions. As plotted in Figure 7, $1/Q^*$ progressively and significantly decreases with increasing temperature. Hence, the surface fractional area of pores must decrease, in agreement with the explanation for the SANS results on interlamellar spacing and temperature. Whether the size of individual pores, the number of pores, or some combination of both is changing cannot be determined in this fashion. Q^* can be related to a surface fractional area of pores upon assuming a particular model of pore morphology.[94,95,117] However, the surface fractional area of pores can be determined in a direct fashion from NMR diffusion measurements on transbilayer diffusion of water,[95] as described next.

^{1}H PFG STE NMR spectra acquired from the same positively magnetically aligned DMPC/DHPC/DMPG ($Q = 5$, $R = 0.1$) bicellar mixture contain a single large spectral signal originating

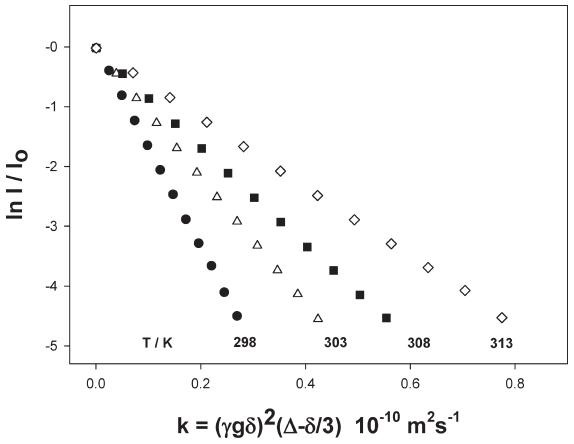

Figure 8. Semilog plot of the integrated intensity of the water resonance in ^{1}H STE PFG NMR spectra of a positively magnetically aligned $Q = 5$, $R = 0.1$ DMPC/DHPC/DMPG bicellar mixture at four different temperatures versus the experimental factor $k = (\gamma\delta g)^2(\Delta - \delta/3)$. The slope in such plots is proportional to the diffusion coefficient D as per eq 10, in this case corresponding to water diffusion in the transbilayer direction. Temperature (K): 298 (●), 303 (△), 308 (■), 313 (◇).

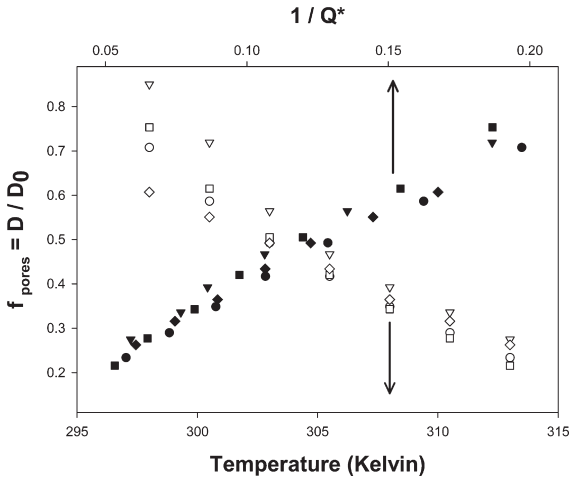

Figure 9. Apparent bilayer pore fraction, $f_{pores} = D/D_0$, from NMR diffusion analysis of transbilayer water diffusion coefficients in positively magnetically aligned DMPC/DHPC/DMPG mixtures at various R = DMPG/DMPC molar ratios as a function of temperature (open symbols), and correlated with the fraction of lipids available to form pores ($1/Q^*$) as derived from ^{31}P NMR chemical shifts for the same mixture at the same temperature (closed symbols). D_0 refers to diffusion coefficient of bulk water at the corresponding temperature. $R = 0.02$ (circles); 0.05 (triangles); 0.10 (squares); 0.15 (tilted squares).

from water. Other resonances, originating with the bicellar lipids, are visible only when the vertical scale is greatly expanded, since these are generally broadened due to residual dipolar interactions so that their intensity is diminished relative to the water resonance upon being subjected to the STE pulse sequence. When the gradient amplitude in the PFG STE NMR pulse sequence is incrementally increased, the resonance intensity decreases in proportion to the diffusion coefficient along the direction of the applied field gradient, in this experiment corresponding to the z-direction parallel to the direction of the main magnetic field. Since the positive magnetic alignment of these bicellar mixtures places the bilayer normal parallel to the main magnetic field direction, the bilayer lamellae lie transverse to the diffusion direction and form a series of barriers to diffusion. The principal pathway for diffusion lies, therefore, through any pores or perforations in these bilayer barriers. Water being small relative to the expected dimension of any pore diameter, its transbilayer diffusion will reflect only the total fractional surface area of pores and not the pore dimensions.

The diffusion coefficient is related to the resonance intensity via eq 10,

$$I = I_0^* \exp\left[-D(\gamma g\delta)^2(\Delta - \delta/3)\right] \qquad (10)$$

where δ (s) is the duration of the square gradient pulse of magnitude g (Tm^{-1}), γ is the magnetogyric ratio, and Δ (s) is the experimental diffusion time.[100] The effects of longitudinal and transverse relaxation are included with I_0^*, the resonance intensity in the absence of any applied field gradient. The apparent diffusion coefficient is obtained from the slope in a plot of $\ln(I/I_0^*)$ versus $k = [(\gamma g\delta)^2(\Delta - \delta/3)]$.

Figure 8 shows such semilogarithm plots for transbilayer water diffusion in positively magnetically aligned DMPC/DHPC/DMPG ($Q = 5$, $R = 0.1$) bicellar mixtures at several different temperatures. Qualitatively, one observes single exponential decays, meaning that a single average diffusion coefficient is sufficient to describe the diffusion of all water molecules. Thus, exchange between environments expected to exhibit different diffusion properties, such as water bound to the lipid bilayer surface versus water resident within bilayer pores versus bulk water in the lamellar interstices, must be fast on the time scale of the diffusion measurement ($\Delta = 100$ ms in this case). At 308 K, the transbilayer water diffusion coefficient is 8×10^{-10} m^2 s^{-1}, or roughly one-third of that of bulk water at the same temperature,[102] demonstrating that the bicellar lamellae significantly obstruct water diffusion in the transbilayer direction. Nevertheless, this diffusion coefficient is far greater than the lamellar limit of $D \sim 10^{-13}$–10^{-14} m^2 s^{-1} expected for near perfect lamellar bilayer sheets,[118,119] which points to the presence of lamellar defects arising from the addition of DHPC. The corresponding root-mean-square displacement, $\langle z^2\rangle^{1/2} = \langle 6D\Delta\rangle^{1/2}$, is on the order of tens of micrometers, equivalent to roughly a thousand interlamellar repeats as measured from SANS data. Hence, the apparent transbilayer water diffusion coefficient represents an average permeation across multiple bilayer barriers.

Quantitatively, Figure 8 shows that the transbilayer water diffusion coefficient decreases with increasing temperature, in direct contrast to the behavior of bulk water, but in agreement with a previous study.[95] Figure 9 shows this in greater detail where the observed transbilayer water diffusion coefficient, normalized with respect to the diffusion coefficient of bulk water at the corresponding temperature, is plotted as a function of temperature for several different DMPG compositions spanning the range $0.02 \le R \le 0.15$. In each case, there is a substantial decrease in the diffusion coefficient with increasing temperature. In the temperature region immediately above the DMPC phase transition (~295 K), there is a considerable range of D/D_0 values as the different DMPG compositions and sample histories influence the precise position and width of this transition as well as the quality of magnetic alignment. However, at temperatures above roughly 300 K, D/D_0 was essentially independent of the DMPG composition in the range investigated. Likewise, the presence or absence of salt (100 mM KCl) made little or no difference.

dx.doi.org/10.1021/la104750x |*Langmuir* 2011, 27, 4838–4847

To explain the counterintuitive temperature dependence of the transbilayer water diffusion in such bicellar mixtures, we link to the behavior of DHPC as deduced from ^{31}P NMR. Previously,[51] it was argued that the relevant physical parameter dictating the transbilayer water diffusion is the relative surface fraction of lamellar versus pore regions, so that a simple relationship pertains between the two, as per eq 11,

$$\frac{D}{D_0} = \frac{1}{1 + \frac{A_{lam}}{A_{perf}}} = f_{pores} \qquad (11)$$

where D_0 is the corresponding diffusion coefficient of bulk water and A_{lam} and A_{perf} are the respective surface areas of lamellar regions and perforations. The fractional surface area of pores is inversely proportional to the fraction of lamellar versus edge lipids as embodied in the ^{31}P NMR-derived quantity Q^*.

Figure 9 shows the relationship between $D/D_0 = f_{pores}$, derived from transbilayer water diffusion data at a particular temperature, and the ^{31}P NMR-derived quantity $1/Q^*$, with the latter being proportional to the fractional surface area of pores, at the same temperature, for various DMPG compositions R = DMPG/DMPC. In all cases, the same correlation between decreasing transbilayer water diffusion and decreasing surface fractional area of pores with increasing temperature is evident. In fact, within the error of the diffusion measurements, there is very little to differentiate the various DMPG compositions from one another, suggesting, again, that the DMPG composition does not particularly influence f_{pores}.

Comparing the surface pore fractional area estimated from SANS and NMR diffusion measurements reveals that values of f_{pores} obtained from NMR diffusion were uniformly greater than those obtained from SANS by roughly a factor of 2, regardless of temperature. For the SANS data, perhaps the greatest source of uncertainty is the value of d_B upon which the estimate of f_{pores} depends and which is obtained by fitting an admittedly simple scattering density model that is more useful for estimating relative changes than absolute values. For the NMR data, perhaps the greatest source of uncertainty is the assumption that water permeation through lamellar regions is negligible, despite the presence of DHPC in such regions. The small differences in the mole fraction of DHPC present in the samples used for NMR versus SANS measurements are certainly insufficient to account for the large differences in calculated values of f_{pores} for the two techniques.

Further to a comparison of SANS-derived and NMR-derived pore fractions, one may calculate the increase in the interstitial volume due to annealing of the bicellar pores with increasing temperature from some initial to some final value using

$$\Delta V_{interstitial}/\text{unit area} = (d - d_b)_{final} - (d - d_b)_{initial} \qquad (12)$$

where d is the interlamellar spacing and d_B is the bilayer thickness. The corresponding loss of volume in the bilayer due to annealing of pores is calculated via

$$\Delta V_{bilayer}/\text{unit area} = (d_B f_{pore})_{final} - (d_B f_{pore})_{initial} \qquad (13)$$

The ratio $\Delta V_{bilayer}/\Delta V_{interstitial}$ permits an evaluation of the reliability of values of f_{pore} derived from SANS and from NMR. For the temperature range between 303 and 313 K, for example, the SANS data yield a ratio $\Delta V_{bilayer}/\Delta V_{interstitial}$ on the order of 0.20, indicating that the apparent decrease in the fraction of pores in the bilayer accounts for only roughly 20% of the increased interstitial volume. For the NMR-derived f_{pore} values, the corresponding ratio is 0.93, showing that the increase in interstitial volume observed via SANS d values is essentially fully accounted for by the decrease in bilayer pore fraction calculated from NMR transbilayer diffusion data.

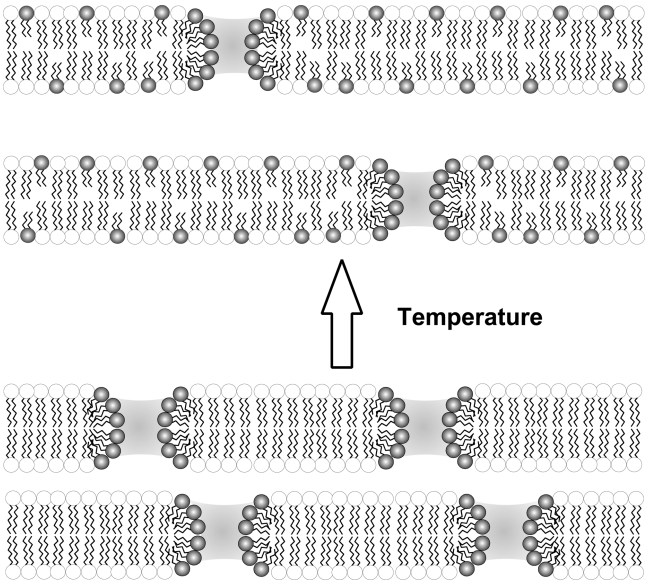

Figure 10. Schematic cross section through a set of stacked perforated lamellae of DMPC/DHPC bicellar mixtures, illustrating temperature effects on morphology. The planar part of the bilayer is composed primarily of the long-chain lipids, DMPC (white), while the curved edges of the pores/perforations are coated with DHPC (black). As temperature increases, DHPC becomes progressively more miscible with DMPC and able to migrate into planar regions, thus reducing the surface fractional area of pores. Consequently, water resident within pores at low temperatures is expelled into the interlamellar regions at higher temperatures, thereby increasing the interlamellar spacing d. As a further consequence, water diffusion in the transbilayer direction is reduced.

CONCLUSIONS

We have provided evidence that the magnetically alignable smectic phase of DMPC/DHPC/DMPG aggregates is made up of perforated lamellae, and that the area fraction of the bilayers occupied by pores decreases with increasing temperature. The thermal evolution of the bilayer's morphology, as deduced from a combination of SANS, ^{31}P NMR, and NMR diffusion observations, is summarized in Figure 10. With increasing T, DHPC molecules are able to migrate from edge regions into lamellar regions, by virtue of their greater miscibility with DMPC at higher temperatures. The resulting decreased pore area fraction produces a concomitantly decreased transbilayer water diffusion coefficient D. The water occupying such pores is squeezed out and forced into the interlamellar region, thereby increasing the interlamellar spacing d.

These findings have potential ramifications both for solution state NMR studies of soluble proteins where bicelles are used as an alignment medium, and for solid state NMR studies of membrane proteins where bicelles are a membrane mimetic. The partial alignment of soluble proteins (and other species) produces residual dipolar couplings (or anisotropic chemical shifts or quadrupolar couplings) which aid in constraining

protein structure models issues, such as relative subdomain orientations in multidomain proteins.[58,61,62,65−67] Critical to such questions is a determination of the magnitude of the asymmetric alignment tensor,[59] which depends on the degree of constraint imposed by the alignment medium and, hence, the spacing between the bicellar lamellae. The counterintuitive effects of temperature on this spacing as found here will be a consideration in such studies, particularly for temperature-dependent dynamics investigations. For solid state NMR studies of membrane protein structure, topology, and dynamics, it is established that bilayer lipid composition influences helical tilt and dynamics,[18] as does any hydrophobic mismatch between protein and bilayer lipids,[33] while the Q ratio specifically influences protein stability, secondary structure, and dynamics.[29] The differential miscibility of DHPC within the planar region of bicelles as a function of temperature will clearly influence such protein properties.

Finally, only a single Q ratio has been investigated here. It would be of importance, clearly, to investigate a range of Q ratios to establish how broadly these phenomena are observable.

AUTHOR INFORMATION

Corresponding Author

*Telephone: 905 828 3805. Fax: 905 828 5425. E-mail: pm.macdonald@utoronto.ca.

ACKNOWLEDGMENT

We thank the Neutron Program for Materials Research (NPMR) for use of the neutron facilities at NRU (Chalk River, Ontario, Canada). J.K. and M.-P.N. acknowledge financial support from the Advanced Foods and Materials Network (Networks of Centers of Excellence) and the NPMR. P.M. thanks the Natural Science and Engineering Research Council (NSERC) of Canada and the University of Toronto for financial support.

REFERENCES

(1) Sanders, C. R.; Hare, B. J.; Howard, K. P.; Prestegard, J. H. *Prog. Nucl. Magn. Reson. Spectrosc.* **1994**, *26*, 421–444.
(2) Sanders, C. R.; Oxenoid, K. *Biochim. Biophys. Acta* **2000**, *1508*, 129–145.
(3) While, J. A.; Deems, R.; Vold, R. R.; Dennis, E. A. *Bioorg. Chem.* **2002**, *30*, 431–442.
(4) Nevzorov, A,A; Mesleh, M. F.; Opella, S. J. *Magn. Reson. Chem.* **2004**, *42*, 162–171.
(5) Sanders, C. R.; Hoffmann, A. K.; Gray, D. N.; Keyes, M. H.; Ellis, C. D. *ChemBioChem* **2004**, *5*, 423–426.
(6) De Angelis, A. A.; Jones, D. H.; Grant, C. V.; Park, S. H.; Mesleh, M. F.; Opella, S. J. *Methods Enzymol.* **2005**, *394*, 350–382.
(7) Marcotte, I.; Auger, M. *Concepts Magn. Reson., A* **2005**, *24A*, 17–37.
(8) Katsaras, J.; Harroun, T. A.; Pencer, J.; Nieh, M. P. *Naturwissenschaften* **2005**, *92*, 355–366.
(9) Sanders, C. R.; Sönnichsen, F. *Magn. Reson. Chem.* **2006**, *44*, S24–S40.
(10) Prosser, R. S.; Evanics, F.; Kitevski, J. L.; Al-Abdul-Wahid, M. S. *Biochemistry* **2006**, *45*, 8453–8465.
(11) Poget, S. F.; Girvin, M. E. *Biochim. Biophys. Acta* **2007**, *1768*, 3098–3106.
(12) Kim, H. J.; Howell, S. C.; Van Horn, W. D.; Jeon, Y. H.; Sanders, C. R. *Prog. Nucl. Magn. Reson. Spectrosc.* **2009**, *55*, 335–360.
(13) Ram, P.; Prestegard, J. H. *Biochim. Biophys. Acta* **1988**, *940*, 289–294.
(14) Sanders, C. R.; Prestegard, J. H. *Biophys. J.* **1990**, *58*, 447–460.
(15) Sanders, C. R.; Schwonek, J. P. *Biochemistry* **1992**, *31*, 8898–8905.
(16) Sanders, C. R.; Landis, G. C. *Biochemistry* **1995**, *34*, 4030–4040.
(17) Drechsler, A.; Separovic, F. *IUBMB Life* **2003**, *55*, 515–523.
(18) Williamson, P. T. F.; Zandomeneghi, G.; Barrantes, F. J.; Watts, A.; Meier, B. H. *Mol. Membr. Biol.* **2005**, *22*, 485–496.
(19) Triba, M. N.; Zoonens, M.; Popot, J. L.; Devaux, P. F.; Warschawski, D. E. *Eur. Biophys. J.* **2006**, *35*, 268–275.
(20) De Angelis, A. A.; Howell, S. C.; Nevzorov, A. A.; Opella, S. J. *J. Am. Chem. Soc.* **2006**, *128*, 12256–12267.
(21) Park, S. H.; De Angelis, A. A.; Nevzorov, A. A.; Wu, C. H.; Opella, S. J. *Biophys. J.* **2006**, *91*, 3032–3042.
(22) De Angelis, A. A.; Opella, S. J. *Nat. Protoc.* **2007**, *2*, 2332–2338.
(23) Nevzorov, A. A.; Park, S. H.; Opella, S. J. *J. Biomol. NMR* **2007**, *37*, 113–116.
(24) Durr, U. H. N.; Yamamoto, K.; Im, S. C.; Waskell, L.; Ramamoorthy, A. *J. Am. Chem. Soc.* **2007**, *129*, 6670–6671.
(25) Park, S. H.; Opella, S. J. *Protein Sci.* **2007**, *16*, 2205–2215.
(26) Muller, S. D.; De Angelis, A. A.; Walther, T. H.; Grage, S. L.; Lange, C.; Opella, S. J.; Ulrich, A. S. *Biochim. Biophys. Acta* **2007**, *1768*, 3071–3079.
(27) Mahalakshmi, R.; Franzin, C. M.; Choi, J.; Marassi, F. M. *Biochim. Biophys. Acta* **2007**, *1768*, 3216–3224.
(28) Durr, U. H. N.; Waskell, L.; Ramamoorthy, A. *Biochim. Biophys. Acta* **2007**, *1768*, 3235–3259.
(29) McKibbin, C.; Farmer, N. A.; Jeans, C.; Reeves, P. J.; Khorana, H. G.; Wallace, B. A.; Edwards, P. C.; Villa, C.; Booth, P. J. *J. Mol. Biol.* **2007**, *374*, 1319–1332.
(30) Mahalakshmi, R.; Marassi, F. M. *Biochemistry* **2008**, *47*, 6531–6538.
(31) Park, S. H.; Loudet, C.; Marassi, F. M.; Dufourc, E. J.; Opella, S. J. *J. Magn. Reson.* **2008**, *193*, 133–138.
(32) Xu, C. Q.; Gagnon, E.; Call, M. E.; Schnell, J. R.; Schwieters, C. D.; Carman, C. V.; Chou, J. J.; Wucherpfennig, K. W. *Cell* **2008**, *135*, 702–713.
(33) Daily, A. E.; Greathouse, D. V.; van der Wel, P. C. A.; Koeppe, R. E. *Biophys. J.* **2008**, *94*, 480–491.
(34) Diller, A.; Loudet, C.; Aussenac, F.; Raffard, G.; Fournier, S.; Laguerre, M.; Grelard, A.; Opella, S. J.; Marassi, F. M.; Dufourc, E. J. *Biochimie* **2009**, *91*, 744–751.
(35) Naito, A. *Solid State Nucl. Magn. Reson.* **2009**, *36*, 67–76.
(36) Cui, T. X.; Canlas, C. G.; Xu, Y.; Tang, P. *Biochim. Biophys. Acta* **2010**, *1798*, 161–166.
(37) Bocharov, E. V.; Pustovalova, Y. E.; Pavlov, K. V.; Volynsky, P. E.; Goncharuk, M. V.; Ermolyuk, Y. S.; Karpunin, D. V.; Schulga, A. A.; Kirpichnikov, M. P.; Efremov, R. G.; Maslennikov, I. V.; Arseniev, A. S. *J. Biol. Chem.* **2007**, *282*, 16256–16266.
(38) Poget, S. F.; Girvin, M. E. *Biochim. Biophys. Acta* **2007**, *1768*, 3098–3106.
(39) Wang, G. S. *Curr Protein Pept. Sci.* **2008**, *9*, 50–69.
(40) Lee, D.; Walter, K. F. A.; Bruckner, A. K.; Hilty, C.; Becker, S.; Griesinger, C. *J. Am. Chem. Soc.* **2008**, *130*, 13822–13823.
(41) Hiller, S.; Wagner, G. *Curr. Opin. Struct. Biol.* **2009**, *19*, 396–401.
(42) Kim, H. J.; Howell, S. C.; Van Horn, W. D.; Jeon, Y. H.; Sanders, C. R. *Prog. Nucl. Magn. Reson. Spectrosc.* **2009**, *55*, 335–360.
(43) Sanders, C. R.; Landis, G. C. *J. Am. Chem. Soc.* **1994**, *116*, 6470–6471.
(44) Struppe, J.; Komives, E. A.; Taylor, S. S.; Vold, R. R. *Biochemistry* **1998**, *37*, 15523–15527.
(45) Losonczi, J. A.; Tian, F.; Prestegard, J. H. *Biochemistry* **2000**, *39*, 3804–3816.
(46) Yu, K.; Kang, S.; Kim, S. D.; Ryu, P. D.; Kim, Y. *J. Biomol. Struct.* **2001**, *18*, 595–606.

(47) Whiles, J. A.; Brasseur, R.; Glover, K. J.; Melacini, G.; Komives, E. A.; Vold, R. R. *Biophys. J.* **2001**, *80*, 280–293.
(48) Glover, K. J.; Whiles, J. A.; Wood, M. J.; Melacini, G.; Komives, E. A.; Vold, R. R. *Biochemistry* **2001**, *40*, 13137–13142.
(49) Marcotte, I.; Dufourc, E. J.; Ouellet, M.; Auger, M. *Biophys. J.* **2003**, *85*, 328–339.
(50) Lindberg, M.; Biverstahl, H.; Graslund, A.; Maler, L. *Eur. J. Biochem.* **2003**, *270*, 3055–3063.
(51) Biverstahl, H.; Andersson, A.; Graslund, A; Maler, L. *Biochemistry* **2004**, *43*, 14940–14947.
(52) Ellena, J. F.; Moulthrop, J.; Wu, J.; Rauch, M.; Jaysinghne, S.; Castle, J. D.; Cafiso, D. S. *Biophys. J.* **2004**, *87*, 3221–3233.
(53) Anderluh, G.; Razpotnik, A.; Podlesek, Z.; Macek, P.; Separovic, F.; Norton, R. S. *J. Mol. Biol.* **2005**, *347*, 27–39.
(54) Dvinskikh, S. V.; Durr, U. H. N.; Yamamoto, K.; Ramamoorthy, A. *J. Am. Chem. Soc.* **2007**, *129*, 794–802.
(55) Al-Abdul-Wahid, M. S.; Neale, C.; Pomes, R.; Prosser, R. S. *J. Am. Chem. Soc.* **2009**, *131*, 6452–6459.
(56) Tjandra, N; Bax, A. *Science* **1997**, *278*, 1111–1114.
(57) Vold, R. R.; Deese, A. J.; Prosser, R. S. *J. Biomol. NMR* **1997**, *9*, 329–335.
(58) Bax, A.; Tjandra, N. *J. Biomol. NMR* **1997**, *10*, 289–292.
(59) Clore, G. M.; Gronenborn, A. M.; Bax, A. *J. Magn. Reson.* **1998**, *133*, 216–221.
(60) Ottiger, M.; Bax, A. *J. Biomol. NMR* **1999**, *13*, 187–191.
(61) Fischer, M. W. F.; Losonczi, J. A.; Weaver, J. L.; Prestegard, J. H. *Biochem.* **1999**, *38*, 9013–9022.
(62) Markus, M. A.; Gerstner, R. B.; Draper, D. E.; Torchia, D. A. *J. Mol. Biol.* **1999**, *292*, 375–387.
(63) Boyd, J.; Redfield, C. *J. Am. Chem. Soc.* **1999**, *121*, 7441–7442.
(64) Cavagnero, S.; Dyson, H. J.; Wright, P. E. *J. Biomol. NMR* **1999**, *13*, 387–391.
(65) Cornilescu, G.; Bax, A. *J. Am. Chem. Soc.* **2000**, *122*, 10143–10154.
(66) Schwalbe, H.; Grimshaw, S. B.; Spencer, A.; Buck, M.; Boyd, J.; Dobson, C. M.; Redfield, C.; Smith, L. J. *Protein Sci.* **2001**, *10*, 677–688.
(67) Ohnishi, S.; Shortle, D. *Proteins: Struct., Funct., Genet.* **2003**, *50*, 546–551.
(68) Luhrs, T. T.; Zahn, R.; Wuthrich, K. *J. Mol. Biol.* **2006**, *357*, 833–841.
(69) Arnold, A.; Labrot, T.; Oda, R.; Dufourc, E. J. *Biophys. J.* **2002**, *83*, 2667–2680.
(70) Van Dam, L.; Karlsson, G.; Edwards, K. *Biochim. Biophys. Acta* **2004**, *1664*, 241–256.
(71) Van Dam, L.; Karlsson, G.; Edwards, K. *Langmuir* **2006**, *22*, 3280–3285.
(72) Rowe, B. A.; Neal, S. L. *Langmuir* **2003**, *19*, 2039–2048.
(73) Ottinger, M.; Bax, A. *J. Biomol. NMR* **1998**, *12*, 361–372.
(74) Raffard, G.; Steinbruckner, S.; Arnold, A.; Davis, J. H.; Dufourc, E. J. *Langmuir* **2000**, *16*, 7655–7662.
(75) Sternin, E.; Nizza, D.; Gawrisch, K. *Langmuir* **2001**, *17*, 2610–2616.
(76) Boltze, J.; Fujisawa, T.; Nagao, T.; Norisada, K.; Saito, H.; Naito, A. *Chem. Phys. Lett.* **2000**, *329*, 215–220.
(77) Luchette, P. A.; Vetman, T. N.; Prosser, R. S.; Hancock, R. E.; Nieh, M. P.; Glinka, C. J.; Krueger, S.; Katsaras, J. *Biochim. Biophys. Acta* **2001**, *1513*, 83–94.
(78) Nieh, M. P.; Ginka, C. J.; Krueger, S.; Prosser, R. S.; Katsaras, J. *Langmuir* **2001**, *17*, 2629–2638.
(79) Nieh, M. P.; Ginka, C. J.; Krueger, S.; Prosser, R. S.; Katsaras, J. *Biophys. J.* **2002**, *82*, 2487–2498.
(80) Nieh, M. P.; Raghunathan, V. A.; Glinka, C. J.; Harroun, T. A.; Pabst, G.; Katsaras, J. *Langmuir* **2004**, *20*, 7893–7897.
(81) Nieh, M.-P.; Raghunathan, V. A.; Glinka, C. J.; Harroun, T. A.; Katsaras, J. *Macromol. Symp.* **2005**, *219*, 135–145.
(82) Harroun, T. A.; Koslowsky, M.; Nieh, M. P.; de Lannoy, C. F.; Raghunathan, V. A.; Katsaras, J. *Langmuir* **2005**, *21*, 5356–5361.
(83) Vold, R. R.; Prosser, R. S. *J. Magn. Reson., Ser. B* **1996**, *113*, 267–271.
(84) Soong, R.; Nieh, M.-P.; Nicholson, E.; Katsaras, J.; Macdonald, P. M. *Langmuir* **2010**, *26*, 2630–2638.
(85) Katsaras, J.; Donaberger, R. L.; Swainson, I. P.; Tennant, D. C.; Tun, Z.; Vold, R. R.; Prosser, R. S. *Phys. Rev. Lett.* **1997**, *78*, 899–902.
(86) Prosser, R. S.; Hunt, S. A.; DiNatale, J. A.; Vold, R. R. *J. Am. Chem. Soc.* **1996**, *118*, 269–270.
(87) Prosser, R. S.; Hwang, J. S.; Vold, R. R. *Biophy. J.* **1998**, *74*, 2405–2418.
(88) Cardon, T. B.; Tiburu, E. K.; Lorigan, G. A. *J. Magn. Reson.* **2003**, *161*, 77–90.
(89) Gaemers, S.; Bax, A. *J. Am. Chem. Soc.* **2001**, *123*, 12343–12352.
(90) Soong, R.; Macdonald, P. M. *Biophys. J.* **2005**, *89*, 1850–1860.
(91) Losonczi, J.; Prestegard, J. H. *J. Biomol. NMR* **1998**, *12*, 447–451.
(92) Crowell, K. J.; Macdonald, P. M. *Biochim. Biophys. Acta* **1999**, *1416*, 21–30.
(93) Nieh, M.-P.; Raghunathan, V. A.; Wang, H; Katsaras, J. *Langmuir* **2003**, *19*, 6936–6941.
(94) Triba, M. N.; Warschawski, D. E.; Devaux, P. E. *Biophys. J.* **2005**, *88*, 1887–1901.
(95) Soong, R.; Macdonald, P. M. *Langmuir* **2009**, *25*, 380–390.
(96) Luzzati, V.; Husson, F *J. Cell. Biol.* **1962**, *12*, 207–219.
(97) Kučerka, N.; Nagle, J. F.; Feller, S. E.; Balgavý, P. *Phys. Rev. E* **2004**, *69*, 051903-1–051903-9.
(98) Nagle, J. F.; Tristram-Nagle, S. *Biochim. Biophys. Acta* **2000**, *1469*, 159–195.
(99) Ammann, C.; Meier, P.; Mebach, A. E. *J. Magn. Reson.* **1982**, *46*, 319–321.
(100) Tanner, J. E. *J. Chem. Phys.* **1970**, *52*, 2523–2526.
(101) Fauth, J. M.; Schweiger, A.; Braunschweiler, L.; Forrer, J.; Ernst, R. R. *J. Magn. Reson.* **1986**, *66*, 74–85.
(102) Mills, R. *J. Phys. Chem.* **1973**, *77*, 685–688.
(103) Pabst, G.; Rappolt, M.; Amenitsch, H.; Bernstorff, S.; Laggner, P. *Langmuir* **2000**, *16*, 8994–9001.
(104) Pabst, G.; Katsaras, J.; Raghunathan, V. A.; Rappolt, M. *Langmuir* **2003**, *19*, 1716–1722.
(105) Nieh, M.-P.; Harroun, T. A.; Raghunathan, V. A.; Glinka, C. J.; Katsaras, J. *Phys. Rev. Lett.* **2003**, *91*, 158105–1 - 158105−9.
(106) Nieh, M.-P.; Harroun, T. A.; Raghunathan, V. A.; Glinka, C. J.; Katsaras, J. *Biophy. J.* **2004**, *86*, 2615–2629.
(107) Helfrich, W. *Z. Naturforsch.* **1975**, *30*, 841–842.
(108) Helfrich, W. *J. Phys. (Paris)* **1985**, *46*, 1263–1268.
(109) Roux, D.; Nallet, F.; Freyssingeas, E.; Porte, G.; Bassereau, P.; Skouri, M.; Marignan, J. *Europhys. Lett.* **1992**, *17*, 575–581.
(110) Schomäcker, R.; Strey, R. *J. Phys. Chem.* **1994**, *98*, 3908–3912.
(111) von Berlepsch, H.; de Vries, R. *Eur. Phys. J. E* **2000**, *1*, 141–152.
(112) Rawicz, W.; Olbrich, K. C.; McIntosh, T.; Needham, D.; Evans, E. *Biophys. J.* **2000**, *79*, 328–339.
(113) Winterhalter, M.; Helfrich, W. *J. Phys. Chem.* **1988**, *92*, 6865–6867.
(114) Mitchell, D. J.; Ninham, B. W. *Langmuir* **1989**, *5*, 1121–1123.
(115) Lekkerkerker, H. N. W. *Physica A* **1990**, *167*, 384–394.
(116) Riske, K. A.; Amaral, L. Q.; Döbereiner, H.-G.; Lamy, M. T. *Biophys. J.* **2004**, *86*, 3722–3733.
(117) Triba, M. N.; Devaux, P. H.; Warschawski, D. E. *Biophys. J.* **2006**, *91*, 1357–1367.
(118) Finkelstein, A. *Water movement through lipid bilayers, pores, and plasma membranes. Theory and reality*; Wiley and Sons: New York, 1987.
(119) Wästerby, P.; Orädd, G.; Lindblom, G. *J. Magn. Res.* **2002**, *157*, 156–159.